AAS 11-502

GRAVITY ERROR COMPENSATION USING SECOND-ORDER GAUSS-MARKOV PROCESSES

Jason M. Leonard[*], Felipe G. Nievinski[†], and George H. Born[‡]

Earth science satellite missions currently require orbit determination solutions with position accuracies to within a centimeter. The estimation of empirical accelerations has become commonplace in precise orbit determination (POD) for Earth-orbiting satellites. Dynamic model compensation (DMC) utilizes an exponentially time-correlated system noise process, known as a first-order Gauss-Markov process (GMP1) to estimate un-modeled accelerations. In this work, we address the use of a second-order Gauss-Markov process to compensate for higher order spherical harmonic gravity accelerations, beyond J_3. Improvements in POD and orbit prediction through the implementation of an optimal GMP2 for empirical acceleration estimation are assessed. The use of a single well calibrated GMP2 outperformes a GMP1 and a poorly calibrated GMP2 for both continuous observations and poor tracking data.

INTRODUCTION

Oceanographic and geodetic Earth science satellite missions currently require orbit determination solutions with position accuracies to within a centimeter.[1] High accuracy requirements demand commensurate mathematical models of orbital dynamics. Regardless of the accuracy of these mathematical models, however, there will always be unknown accelerations acting upon a spacecraft. The estimation of empirical accelerations has become commonplace in precise orbit determination (POD) for Earth-orbiting satellites.[1,2,3]

Empirical acceleration estimation methods are more commonly known as reduced dynamic modeling (RDM).[2,3] Several methods exist to estimate these un-modeled accelerations. One such method attempts to estimate periodic accelerations with trigonometric coefficients at fixed frequencies.[1,4] Another, called dynamic model compensation (DMC), utilizes an exponentially time-correlated system noise process, known as a first-order Gauss-Markov process (GMP1).[5,6] As an initial proof-of-concept, Reference 7 demonstrated an improvement in POD through the use of a second-order Gauss-Markov process (GMP2) for modeling J_3 gravity. This was made possible by the fact that GMP2 allow for a more flexible auto-covariance model with both exponential decay and sinusoidal oscillation properties. Due to the flexible auto-covariance model, GMP2 can be used to more accurately model a variety of accelerations that tend to repeat as function of satellite orbital revolution, such as gravity, atmospheric drag, and solar radiation pressure.

In this work, several GMP methods are compared for compensating higher order spherical harmonic gravity accelerations, beyond J_2. A derivation of GMPs is also provided. Secondly, position

[*]Graduate Research Assistant, Department of Aerospace Engineering, University of Colorado, Boulder, CO 80309-0431
[†]Ph.D. student, Department of Aerospace Engineering, University of Colorado, Boulder, CO 80309-0431
[‡]Professor, Department of Aerospace Engineering Sciences and Director, Colorado Center for Astrodynamics Research, University of Colorado, Boulder, CO 80309-0431

and acceleration estimation results are presented for two orbits over two different tracking regimes. Thirdly, an introduction to compound GMP2 is presented, as used for gravity error compensation.

FILTER THEORY

Sequential Filter

For completeness, we repeat the derivation found in Reference 7. The state vector is denoted by $\mathbf{X}(t)$ and contains the satellites position and velocity coordinates as well as parameters governing accelerations acting on the satellite such as gravity and atmospheric drag coefficient. The dynamic model and observation model are respectively

$$\dot{\mathbf{X}}(t) = \mathbf{F}(\mathbf{X}, t), \tag{1}$$

$$\mathbf{Y}(t) = \mathbf{G}(\mathbf{X}, t). \tag{2}$$

These models are then linearized about their reference trajectory (denoted with a *) by

$$\dot{\mathbf{x}}(t) = \mathbf{A}(t)\mathbf{x}(t) + \mathbf{B}(t)\mathbf{n}(t), \tag{3}$$

$$\mathbf{y}(t) = \tilde{\mathbf{H}}(t)\mathbf{x}(t) + \boldsymbol{\epsilon}(t), \tag{4}$$

where $\mathbf{x}(t) = \mathbf{X}^*(t) - \mathbf{X}(t)$ and $\dot{\mathbf{x}}(t) = \dot{\mathbf{X}}^*(t) - \dot{\mathbf{X}}(t)$. Here, $\mathbf{n}(t)$ and $\boldsymbol{\epsilon}(t)$ are the dynamic and observation noise, respectively, and $\mathbf{B}(t)$ is the process noise mapping matrix. The matrix $\mathbf{A}(t)$ is evaluated along the reference trajectory $\mathbf{X}^*(t)$ and is given by

$$\mathbf{A}(t) = \frac{\partial \mathbf{F}(\mathbf{X}^*, t)}{\partial \mathbf{X}}. \tag{5}$$

The state transition matrix $\Phi(t, t_0)$ and is related to $\mathbf{A}(t)$ by

$$\dot{\Phi}(t, t_0) = \mathbf{A}(t)\Phi(t_0, t_0). \tag{6}$$

The observation-state mapping matrix is thus given by

$$\tilde{\mathbf{H}}(t) = \frac{\partial \mathbf{G}(\mathbf{X}^*, t)}{\partial \mathbf{X}}, \tag{7}$$

where $\mathbf{G}(\mathbf{X}^*, t)$ are the observation-state relationships evaluated on the reference trajectory.

Shaping Filter

There are many cases in which a commonly employed white Gaussian noise model does not describe the system dynamic noise adequately. It would be more desirable to have a model that could match the empirical auto-covariance or power spectral density data of an observed system, and then generate a stochastic mathematical model to reproduce the empirical characteristics. If an observed set of data were samples of a stationary Gaussian process with known auto-covariance (or power spectral density), then a linear time-invariant system, or shaping filter, driven by white Gaussian noise, could provide such a model.[8] Moreover, it is often the case that only the first and second order statistics are known, for which a Gaussian process with the same first and second order statistics can be generated by a shaping filter.

We previously defined our system dynamics by Eq. (3) and Eq. (4) where the observation noise $\boldsymbol{\epsilon}(t)$ is postulated uncorrelated and the dynamic noise $\mathbf{n}(t)$ is a non-white, time-correlated, dynamic Gaussian noise. The latter is obtained by passing a white Gaussian noise, $\mathbf{w}(t)$, through a shaping filter defined by

$$\dot{\mathbf{x}}_{\mathrm{s}}(t) = \mathbf{A}_{\mathrm{s}}(t)\mathbf{x}_{\mathrm{s}}(t) + \mathbf{B}_{\mathrm{s}}(t)\mathbf{w}(t), \tag{8}$$

$$\mathbf{y}_{\mathrm{s}}(t) = \tilde{\mathbf{H}}_{\mathrm{s}}(t)\mathbf{x}_{\mathrm{s}}(t), \tag{9}$$

where the shaping filter output, $\mathbf{y}_{\mathrm{s}}(t) = \mathbf{n}(t)$, is used to drive the system defined by Eq. (3). An augmented state vector $\mathbf{x}_{\mathrm{a}}(t)$ is then defined through

$$\mathbf{x}_{\mathrm{a}}(t) = \begin{bmatrix} \mathbf{x}(t) \\ \mathbf{x}_{\mathrm{s}}(t) \end{bmatrix}, \tag{10}$$

where the augmented state equation is given by

$$\begin{bmatrix} \dot{\mathbf{x}}(t) \\ \dot{\mathbf{x}}_{\mathrm{s}}(t) \end{bmatrix} = \begin{bmatrix} \mathbf{A}(t) & \mathbf{B}(t)\tilde{\mathbf{H}}_{\mathrm{s}}(t) \\ \mathbf{0} & \mathbf{A}_{\mathrm{s}}(t) \end{bmatrix} \begin{bmatrix} \mathbf{x}(t) \\ \mathbf{x}_{\mathrm{s}}(t) \end{bmatrix} + \begin{bmatrix} \mathbf{0} \\ \mathbf{B}_{\mathrm{s}}(t) \end{bmatrix} \mathbf{w}(t), \tag{11}$$

or

$$\dot{\mathbf{x}}_{\mathrm{a}}(t) = \mathbf{A}_{\mathrm{a}}(t)\mathbf{x}_{\mathrm{a}}(t) + \mathbf{B}_{\mathrm{a}}(t)\mathbf{w}(t), \tag{12}$$

and its associated output equation

$$\begin{aligned} \mathbf{y}_{\mathrm{a}}(t) &= \begin{bmatrix} \tilde{\mathbf{H}}(t) & \mathbf{0} \end{bmatrix} \begin{bmatrix} \mathbf{x}(t) \\ \mathbf{x}_{\mathrm{s}}(t) \end{bmatrix} + \boldsymbol{\epsilon}(t), \\ &= \tilde{\mathbf{H}}_{\mathrm{a}}(t) \quad \mathbf{x}_{\mathrm{a}}(t) + \boldsymbol{\epsilon}(t). \end{aligned} \tag{13}$$

Time Update

The previous section developed a set of equations for a linear stochastic system driven by white noise and defined by Eq. (12). It is possible to interpret it as a linear stochastic differential equation of the form

$$d\mathbf{x}_{\mathrm{a}}(t) = \mathbf{A}_{\mathrm{a}}(t)\mathbf{x}_{\mathrm{a}}(t)dt + \mathbf{B}_{\mathrm{a}}(t)d\mathbf{w}(t), \tag{14}$$

whose solution is

$$\mathbf{x}_{\mathrm{a}}(t) = \Phi_{\mathrm{a}}(t, t_0)\mathbf{x}_{\mathrm{a}}(t_0) + \int_{t_0}^{t} \Phi_{\mathrm{a}}(t, t')\mathbf{B}_{\mathrm{a}}(t')d\mathbf{w}(t'), \tag{15}$$

where $\Phi_{\mathrm{a}}(t, t_0) = \partial\mathbf{X}_{\mathrm{a}}(t)/\partial\mathbf{X}_{\mathrm{a}}(t_0)$ and the statistical expectation $\mathrm{E}\{\mathbf{x}_{\mathrm{a}}(t)\} = 0$. Also, the stochastic integral of the white Gaussian noise process is implicitly independent of $\mathbf{x}_{\mathrm{a}}(t)$ and therefore,

$$\mathrm{E}\left\{ \left[\int_{t_0}^{t} \Phi_{\mathrm{a}}(t, t')\mathbf{B}_{\mathrm{a}}(t')d\mathbf{w}(t') \right] [\mathbf{x}_{\mathrm{a}}(t)] \right\} = 0, \tag{16}$$

thus the time update for the state $\mathbf{x}_{\mathrm{a}}(t)$ is not affected and is simply $\mathbf{x}_{\mathrm{a}}(t) = \Phi_{\mathrm{a}}(t, t_0)\mathbf{x}_{\mathrm{a}}(t_0)$. However, the variance-covariance matrix of $\mathbf{x}_{\mathrm{a}}(t)$ is affected and has the form

$$\bar{\mathbf{P}}_{\mathrm{a}}(t) = \Phi_{\mathrm{a}}(t, t_0)\mathbf{P}_{\mathrm{a}}(t_0)\Phi_{\mathrm{a}}^{\mathrm{T}}(t, t_0) + \int_{t_0}^{t} \Phi_{\mathrm{a}}(t, t')\mathbf{B}_{\mathrm{a}}(t')\mathbf{Q}_{\mathrm{a}}(t')\mathbf{B}_{\mathrm{a}}^{\mathrm{T}}(t')\Phi_{\mathrm{a}}^{\mathrm{T}}(t, t')dt', \tag{17}$$

$$\dot{\mathbf{P}}_{\mathrm{a}}(t) = \mathbf{A}_{\mathrm{a}}(t)\bar{\mathbf{P}}_{\mathrm{a}}(t) + \bar{\mathbf{P}}_{\mathrm{a}}(t)\mathbf{A}_{\mathrm{a}}^{\mathrm{T}}(t) + \mathbf{B}_{\mathrm{a}}(t)\mathbf{Q}_{\mathrm{a}}(t)\mathbf{B}_{\mathrm{a}}^{\mathrm{T}}(t). \tag{18}$$

This relationship allows for a time-varying system model and non-white, time-correlated, dynamic Gaussian noise model to be evaluated. Two possible methods of solution exist for non-trivial dynamics: numerical integration of Eq. (18); or a discrete case for time-invariant or slowly varying system models based on Eq. (17). For the derivation of the discrete case we following closely Reference 8:

$$\bar{\mathbf{P}}_{\mathrm{a}}(t) = \Phi_{\mathrm{a}}(t, t_0)\mathbf{P}_{\mathrm{a}}(t_0)\Phi_{\mathrm{a}}^{\mathrm{T}}(t, t_0) + \mathbf{B}_{\mathrm{d}}(t_0)\mathbf{Q}_{\mathrm{d}}(t_0)\mathbf{B}_{\mathrm{d}}^{\mathrm{T}}(t_0), \tag{19}$$

where the subscript "d" denotes the discrete case to distinguish it from the instantaneous case previously presented (see Appendix B for matrices $\mathbf{B}_{\mathrm{d}}$ and $\mathbf{Q}_{\mathrm{d}}$). If the system model natural transients are time-invariant or slowly varying when compared to the observation samples, then a first order approximation can be used, where

$$\Phi_{\mathrm{a}}(t, t_0) = \mathbf{I} - \mathbf{A}_{\mathrm{a}}(t_0) \times (t - t_0), \tag{20}$$

$$\mathbf{Q}_{\mathrm{d}}(t_0) = \mathbf{B}_{\mathrm{a}}(t_0)\mathbf{Q}_{\mathrm{a}}(t_0)\mathbf{B}_{\mathrm{a}}^{\mathrm{T}}(t_0) \times (t - t_0). \tag{21}$$

GAUSS-MARKOV THEORY

A Gauss-Markov random process is a Markov random process with restriction that the probability $p[x(t)]$ and the conditional probability $p[x(t)/x(t+\tau)]$, where $\tau = \Delta t$, are Gaussian density functions for all times t and $t + \tau$ over the interval $t_0 \rightarrow t_f$.[9] In terms of filter theory, a zeroth-, first-, and second-order process (GMP0, GMP1, GMP2) augment the state vector with zero, one, or two parameters, respectively, per spatial dimension.[7] For any scalar process zero-mean noise the auto-covariance is defined as

$$\Psi_{nn}(\tau) = \mathrm{E}\{n(t)n(t+\tau)\}; \tag{22}$$

Pure white noise is defined by a GMP0 whose auto-covariance function is represented by

$$\Psi_{nn}(\tau) = \sigma^2\delta(\tau), \tag{23}$$

where σ^2 is the noise variance corresponding to $\tau = 0$ and δ is the Dirac delta function. GMP1 is defined by an exponentially correlated function with a correlation time T, where $\lambda = 1/T$, and an auto-covariance

$$\Psi_{nn}(\tau) = \sigma^2 e^{-\lambda\tau}. \tag{24}$$

GMP1 is also defined by the first-order Langevin equation of the form*

$$\dot{n}(t) = -\lambda n(t) + w(t), \tag{25}$$

$$\mathrm{E}\{w(t)\} = 0, \quad \mathrm{E}\{w(t)w(t+\tau)\} = Q\delta(\tau). \tag{26}$$

*It must be made aware that Q in Eq. (26) and q in Eq. (28) are the strengths of a white noise process but may have different units and are thus defined differently. Also σ^2 in Eq. (23) $\neq Q$ or q but can also be defined as the strength of a white noise process for GMP0.

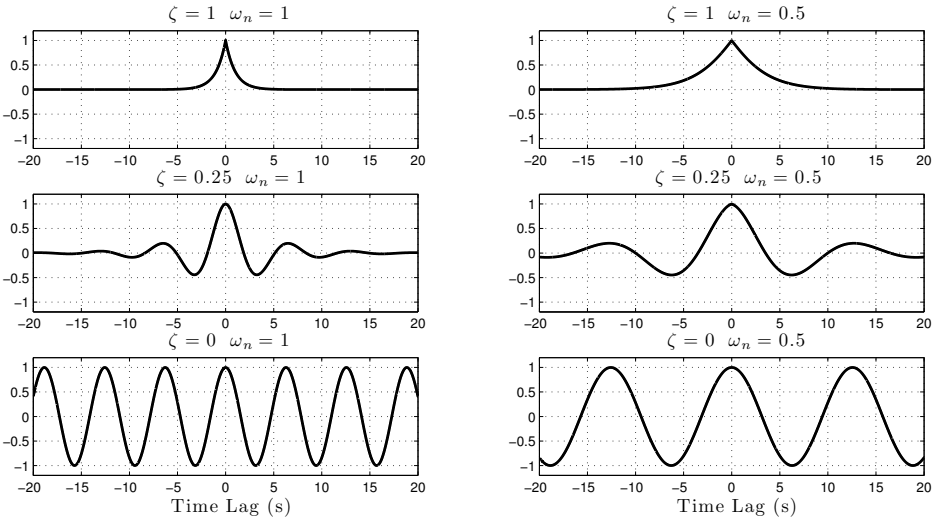

Figure 1. Auto-covariance functions for different instances of second-order GMP (source: Reference 7).

The second-order Gauss-Markov process is defined by an autnomous second-order dynamical system with a white noise forcing function of the type:*

$$\begin{bmatrix}\dot{x}_1\\ \dot{x}_2\end{bmatrix} = \begin{bmatrix}0 & 1\\ -\omega_n^2 & -2\zeta\omega_n\end{bmatrix}\begin{bmatrix}x_1\\ x_2\end{bmatrix} + \begin{bmatrix}0\\ c\end{bmatrix} w(t), \tag{27}$$

$$\mathrm{E}\{w(t)\} = 0, \quad \mathrm{E}\{w(t)w(t+\tau)\} = q\delta(\tau), \tag{28}$$

where ω_n, ζ, and c are constants.† The strength of the white noise process is generally taken to be $q = 1$ and can be increased to add more noise. The state transition matrix for Eq. (27) is easily obtained:

$$\Phi_s(t) = e^{-\zeta\omega_n t}\begin{bmatrix}\cos\beta t + \dfrac{\zeta\omega_n}{\beta}\sin\beta t & \dfrac{1}{\beta}\sin\beta t\\ -\dfrac{\omega_n^2}{\beta}\sin\beta t & \cos\beta t - \dfrac{\zeta\omega_n}{\beta}\sin\beta t\end{bmatrix}, \tag{29}$$

where, $\beta = \omega_n\sqrt{1-\zeta^2}$. From Eq. (17) with $\mathbf{B}_\mathrm{s} = [\,0,\ c\,]^\mathsf{T}$, the auto-covariance function for a GMP2 is given by[9,10]

$$\Psi_{nn}(\tau) = \sigma^2 e^{-\zeta\omega_n|\tau|}\left\{\cos\beta|\tau| + \frac{\zeta\omega_n}{\beta}\sin\beta|\tau|\right\}, \tag{30}$$

where $\sigma^2 = qc^2/4\omega_n^3\zeta$ (see Appendix A for details). This formula will always be written for the underdamped case; for the aperiodic case let $\beta \to 0$ and for the overdamped case set $\beta = \mathrm{i}\beta$.[10]

Figure 1 illustrates the versatility of the GMP2 auto-covariance function as see in Eq. (30). From GMP2, we can obtain GMP0, GMP1 and a pure sinusoid by altering the coefficients ω_n, and ζ. For

*Notice that Reference 7 followed Reference 8, yet here we follow Reference 9 and Reference 10; these two are not exactly equivalent especially in Eq. (27), (30), and (53). Furthermore, there was a typo in Reference 7, Eq. (16): where it is b, but should be c.

†In Reference 7, $\omega_n = \omega$ and c is a variable different than the constant defined here.

example, if $\zeta = 1$, it degenerates into GMP1 with a pure exponential decay. On the other extreme, $\zeta = 0$ leads to a pure sinusoidal oscillation. The frequencies are governed by ω_n and if $\zeta = 1$ with $\omega_n \to \infty$, we approach the solution for GMP0.

METHOD

A set of range and range-rate observations are generated from a space-borne geostationary (GEO) tracking network (three GEO tracking satellites seperated by 120°) using true equations of motion that are corrupted by white, Gaussian noise with a standard deviation of 0.1 m and 0.01 m/s, respectively. An estimate of the true state of the satellite is obtained by an inversion of such simulated observations through a conventional Kalman filter. Spacecraft state vector is expressed in an Earth-centered inertial (ECI) coordinate system, where the X-Y plane coincides with the Earth equatorial plane, and the X- and Z- axes directed toward the mean equinox and north pole, respectively.

Simulated true equations of motion are integrated with an efficient seventh-order Ruge-Kutta-Fehlberg RKF7(8) algorithm.[11] The true equations of motion include acceleration of the Earth's spherical and nonspherical gravitational field, as well as atmospheric drag. The evaluation of Earth's gravitational acceleration is taken from the GRACE gravity model (GGM02C)[12] for spherical harmonic terms up to degree 100 and order 100 using the normalized Cartesian model.[13] A simple drag model with spherical body was used. The atmospheric density is given by the US Naval Research Laboratory Mass Spectrometer and Incoherent Scatter Radar (NRLMSISE-00) model.[14]

Filter equations of motion consist of Earth central-body and oblateness (J_2) with atmospheric drag and a term for un-modeled accelerations (expressed as either a GMP1 or GMP2). The reduced filter equations of motion provide a mismatch in the dynamic model between the filter and truth allowing for GMPs to compensate for the dynamical model errors and recover the higher order gravity harmonics (see Appendix B for filter implementation). Calibration for the GMP coefficients σ^2, ω_n, and ζ is done using the method presented in Reference 7.

For completeness, here we briefly review the calibration method presented in Reference 7. It must be assumed that the GMP coefficients (σ^2, ζ, and ω_n in Eq. (30)) are known during the filter runs. Calibrating such coefficients can be a problem and is addressed in a three-step procedure: (a) obtain sample accelerations; (b) form covariances; and (c) fit the auto-covariance model to the samples. The method of calibration or tuning presented here is commonly addressed as "adaptive filtering or estimation."[15,16,17,18] Please refer to Reference 7 for a complete assessment of the calibration method used in this work.

Two low Earth orbit (LEO) cases were considered: Case 1 is an eccentric orbit with a perigee/apogee height of 160/380 km, an inclination of 110°, argument of perigee of 130°, and an orbital period of about 90 min; and Case 2 is a 1335 km near circular orbit with an inclination of 66.03°, argument of perigee of 23°, and an orbital period of about 112 min. Case 1 experiences a highly variable acceleration and auto-covariance function and is a typical LEO satellite. Case 2 is based on a Jason-1 type orbit in which the auto-covariance function is expected to exhibit less variability.

RESULTS

Position and acceleration estimation results are presented for two cases over two different tracking regimes: constant tracking every 10 seconds; and random loss of tracking 90% of the time. Prior to filter convergence, the first 1000 seconds of every filter run is ignored when computing the statistics.

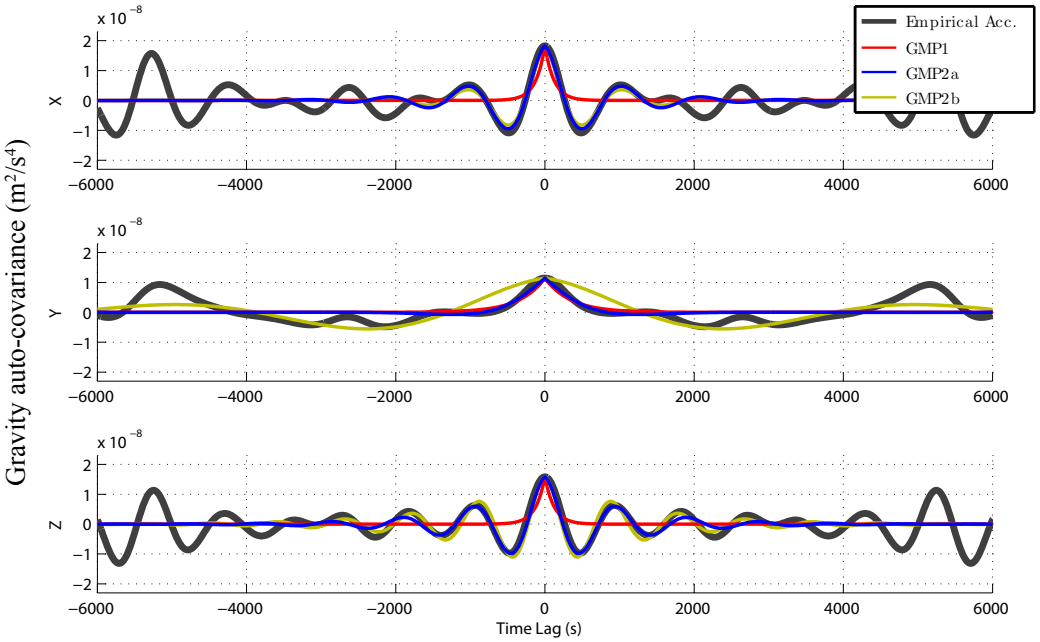

Figure 2. Case 1 acceleration auto-covariance (gray) with GMP1 (red), restrained GMP2a (blue) and unrestrained GMP2b (gold) fits.

Case 1

A single GMP1 and two individual GMP2s (restrained GMP2a and unrestrained GMP2b) are fit to the auto-covariance of estimated un-modeled accelerations as seen in Figure 2 from an initial filter calibration run. A restrained auto-covariance fit models only small time-lags, whereas, an unrestrained fit tries to model larger time-lags. Figure 3 shows filtered acceleration results for a period of constant tracking. Both GMP1 and GMP2 follow the actual acceleration closely.

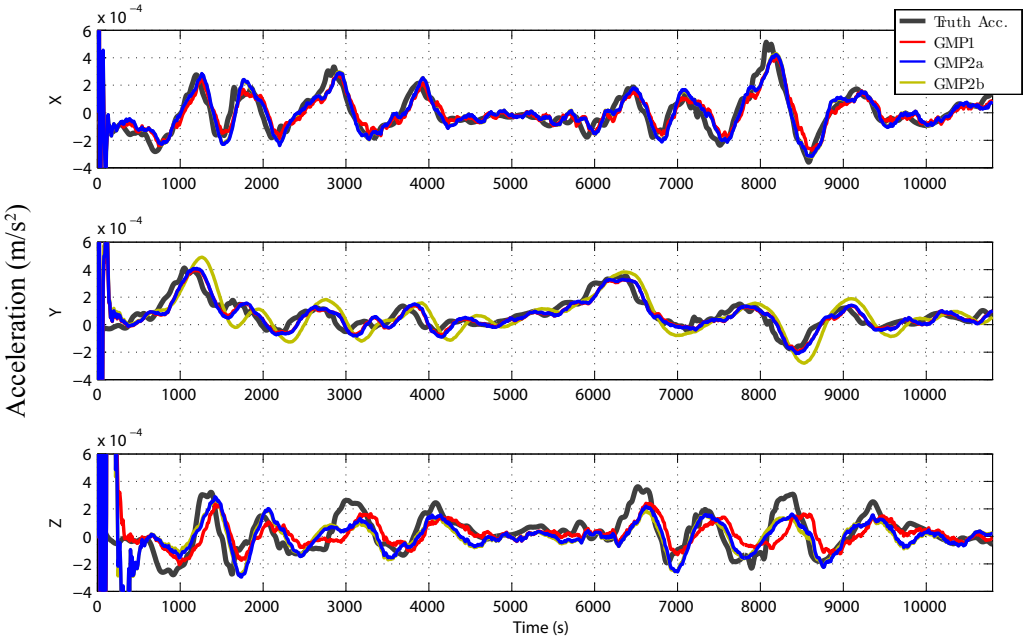

Figure 3. Case 1 acceleration for fully observed filter run.

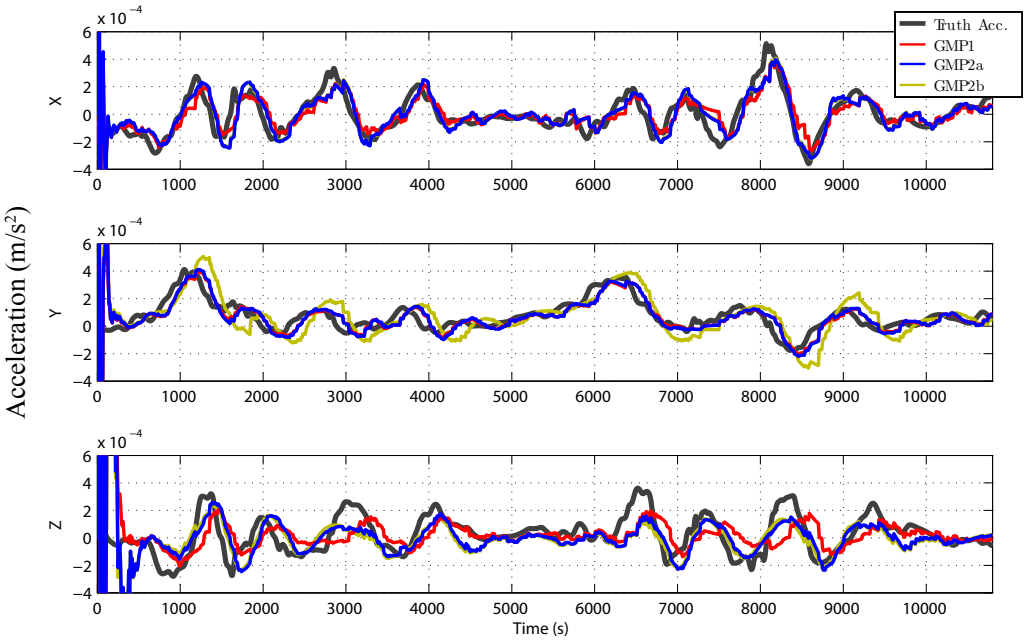

Figure 4. Case 1 acceleration for partially observed filter run.

Table 1 summarizes the statistics for this filter run. GMP2 outperforms GMP1 by up to 35%. The GMP2b Y coordinate estimation is the worst and can be explained by the poor unrestrained fit near the origin of the auto-covariance as seen in Figure 2. A better fit is obtained by restraining the calibration of the GMP2 for an optimal fit near the origin instead of attempting to pick up all transients over the full time lag. Here we have forced the GMP2a auto-covariance model to be optimal on the interval of $|\tau| \leq 2{,}000$ s. This is an important lesson when compared to previous work (Reference 7), where it was unclear whether preference should be given to fitting the most variance under the empirical auto-covariance function instead of only near the origin.

Table 1. Case 1 fully observed period filter RMS Values. RMS values are computed from the difference between filtered estimates and true un-modeled accelerations. Percent change is calculated as GMP (RMS2 - RMS1)/RMS1.

	Position (m)					Acceleration (μm/s^2)				
	GMP1	GMP2a	%a	GMP2b	%b	GMP1	GMP2a	%a	GMP2b	%b
X	0.0756	0.0675	-11%	0.0682	-10%	68.113	55.031	-19%	54.563	-20%
Y	0.0788	0.0732	-7%	0.2232	183%	44.501	42.714	-4%	73.633	65%
Z	0.8651	0.5638	-35%	0.5757	-33%	117.32	84.152	-28%	87.393	-26%
R	0.8720	0.5726	-34%	0.6212	-28%	142.77	109.25	-23%	126.63	-11%

Another filter run is executed as seen in Figure 4 in which a random loss of tracking throughout the data arc exists. Table 2 summarizes the statistics for this period. Again, GMP2a outperforms GMP1 and GMP2b in acceleration. The Y coordinate for GMP2b remains limited by the auto-covariance fit near the origin. The Y coordinate is challenging even for GMP2a because the empirical auto-covariance dies off without the oscillations exhibited in the X and Z coordinates.

Table 2. Case 1 partially observed period filter RMS Values. RMS values are computed from the difference between filtered estimates and true un-modeled accelerations. Percent change is calculated as GMP (RMS2 - RMS1)/RMS1.

	Position (m)					Acceleration (μm/s^2)				
	GMP1	GMP2a	%a	GMP2b	%b	GMP1	GMP2a	%a	GMP2b	%b
X	0.2056	0.1694	-18%	0.1654	-20%	76.970	68.124	-11%	67.965	-12%
Y	0.1525	0.1634	7%	0.4762	212%	49.320	51.310	4%	89.679	82%
Z	1.3447	0.9626	-28%	0.9527	-29%	119.120	95.885	-20%	99.287	-17%
R	1.3688	0.9909	-28%	1.0779	-21%	150.160	128.33	-15%	150.06	-1%

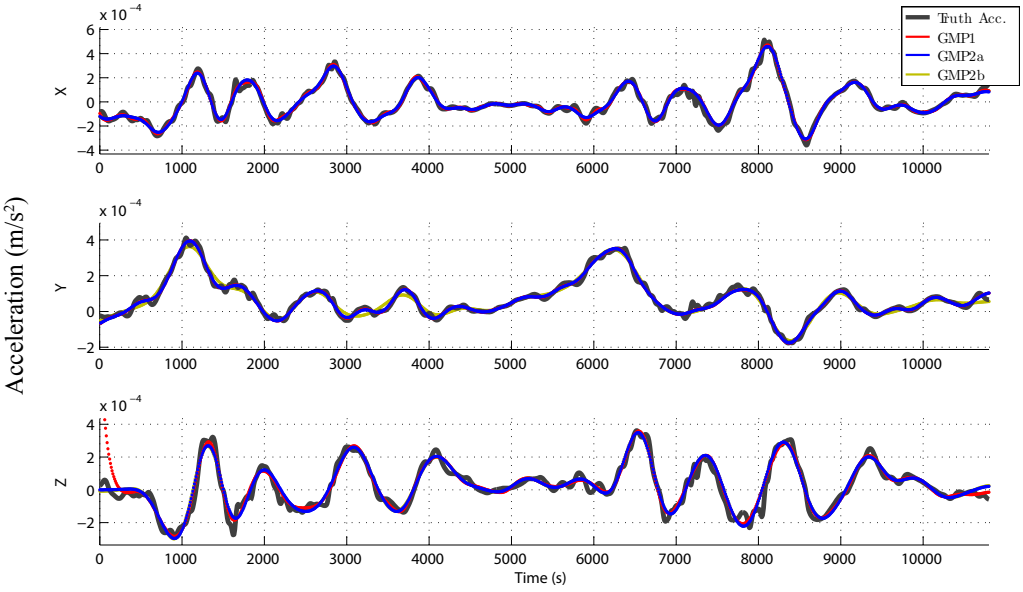

Figure 5. Case 1 acceleration for fully observed smoothed run.

Case 1 is then backward smoothed to determine how well the un-modeled accelerations could be recovered. Figure 5 shows the smoother results for the fully observed case 1 filter run. All three methods recover the un-modeled accelerations rather well while GMP2b is the worst in the Y coordinate. Table 3 displays the statistics for the smoothing run. One can see that smoothing has greatly increased the recovery of un-modeled accelerations for case 1. In this case there is no benefit in using GMP2 in a smoothing run.

Table 3. Case 1 fully observed period smoothed RMS Values. RMS values are computed from the difference between filtered estimates and true un-modeled accelerations. Percent change is calculated as GMP (RMS2 - RMS1)/RMS1.

	Position (m)					Acceleration (μm/s^2)				
	GMP1	GMP2a	%a	GMP2b	%b	GMP1	GMP2a	%a	GMP2b	%b
X	0.0235	0.0300	28%	0.0299	27%	18.391	20.601	12%	20.274	10%
Y	0.0312	0.0359	15%	0.1176	277%	12.258	12.909	5%	19.170	56%
Z	0.3132	0.3171	1%	0.3135	0%	28.590	31.742	11%	31.947	12%
R	0.3156	0.3205	2%	0.3361	7%	36.137	39.983	11%	42.416	17%

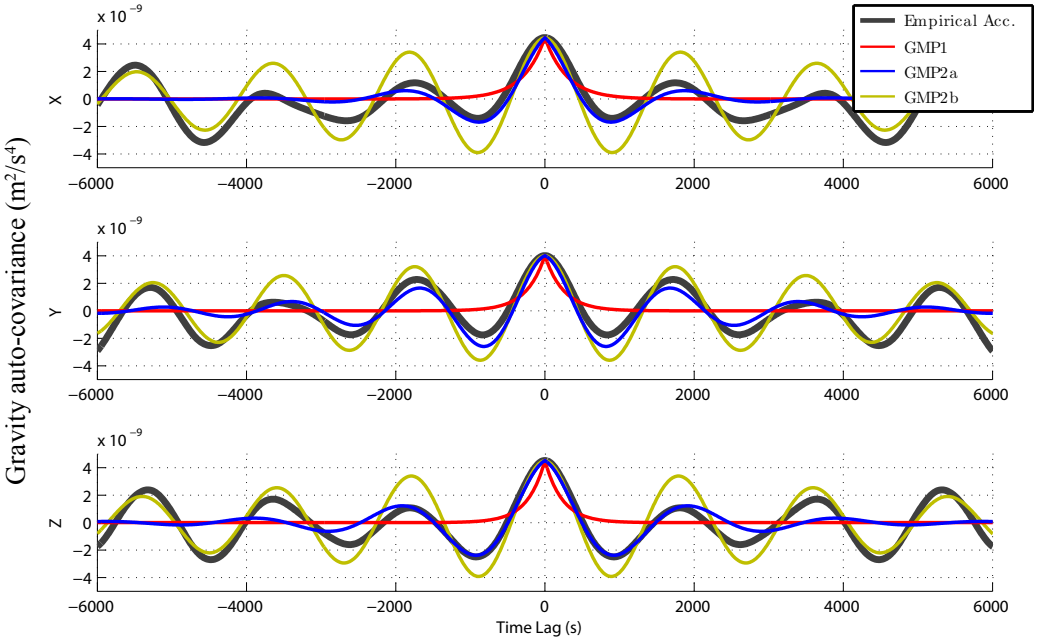

Figure 6. Case 2 acceleration auto-covariance (gray) with GMP1 (red), restrained GMP2a (blue) and unrestrained GMP2b (gold) fits.

Case 2

Similar to case 1 a single GMP1 and two individual GMP2s (restrained GMP2a and unrestrained GMP2b) are fit to the auto-covariance of estimated un-modeled acceleration as seen in Figure 6 from an initial filter calibration run. Here the difference between GMP2a and GMP2b is more drastic in all coordinates. Figure 7 shows filtered acceleration results for a period of constant tracking. Again, both GMP1 and GMP2 follow the actual acceleration closely.

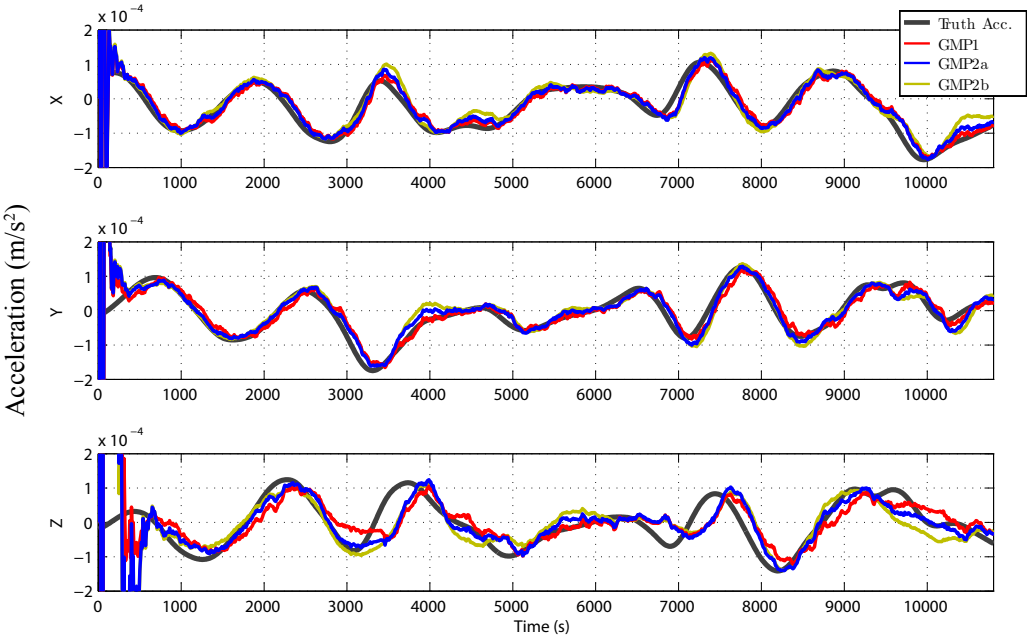

Figure 7. Case 2 acceleration for fully observed filter run.

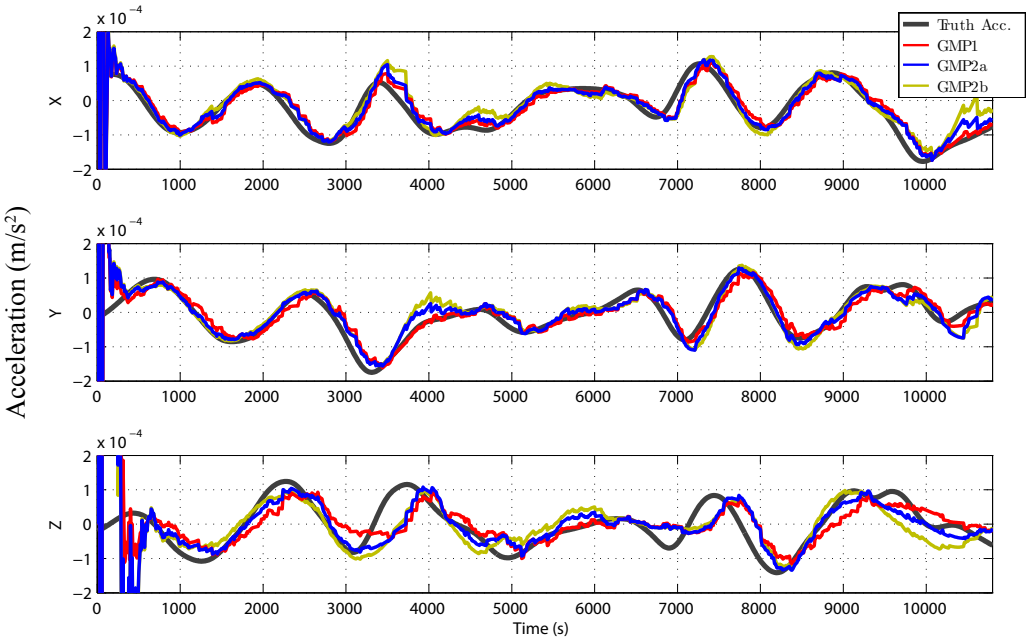

Figure 8. Case 2 acceleration for partially observed filter run.

Table 4 summarizes the statistics for this. Again, here we have forced the GMP2a auto-covariance model to be optimal on the interval of $|\tau| \leq 2{,}000$ s. The GMP2b auto-covariance fit is over the interval of $|\tau| \leq 10{,}000$ s attempting to recovery all transients; this actually does harm to the filter. GMP2a outperforms GMP1 and GMP2b in position and acceleration in all coordinates.

Table 4. Case 2 fully observed period filter RMS Values. RMS values are computed from the difference between filtered estimates and true un-modeled accelerations. Percent change is calculated as GMP (RMS2 - RMS1)/RMS1.

	Position (m)					Acceleration (μm/s^2)				
	GMP1	GMP2a	%a	GMP2b	%b	GMP1	GMP2a	%a	GMP2b	%b
X	0.0631	0.0520	-18%	0.0815	29%	21.932	17.933	-18%	25.264	15%
Y	0.0606	0.0561	-7%	0.0824	35%	21.260	17.415	-18%	22.748	7%
Z	0.6745	0.5110	-24%	0.8200	22%	44.813	38.518	-14%	43.477	3%
R	0.6801	0.5167	-24%	0.8282	22%	54.233	45.918	-15%	55.190	2%

Another filter run is executed as seen in Figure 8 in which a random loss of tracking throughout the data arc exists. Table 5 summarizes the statistics for this period. For this case, GMP2a outperforms GMP1 and GMP2b in all coordinates. Again, the Y coordinate of GMP2b is limited by the auto-covariance fit near the origin.

Table 5. Case 2 partially observed period filter RMS Values. RMS values are computed from the difference between filtered estimates and true un-modeled accelerations. Percent change is calculated as GMP (RMS2 - RMS1)/RMS1.

	Position (m)					Acceleration (μm/s^2)				
	GMP1	GMP2a	%a	GMP2b	%b	GMP1	GMP2a	%a	GMP2b	%b
X	0.1394	0.1124	-19%	0.2025	45%	28.036	23.381	-17%	33.320	18%
Y	0.1319	0.1204	-9%	0.1590	21%	26.660	22.607	-15%	28.482	7%
Z	0.9219	0.7264	-21%	1.3781	50%	50.070	42.325	-15%	47.641	5%
R	0.9417	0.7448	-21%	1.4020	49%	63.275	53.378	-15%	64.739	2%

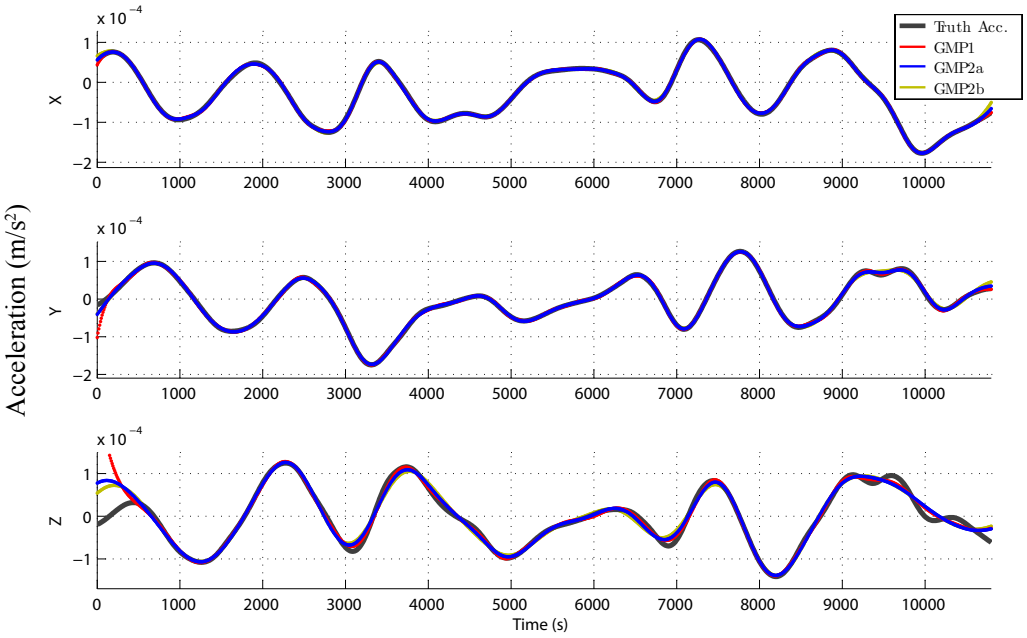

Figure 9. Case 2 acceleration for fully observed smoothed run.

Case 2 is then backward smoothed to determine how well the un-modeled accelerations could be recovered. Figure 9 shows the smoother results for the fully observed case 2 filter run. All three methods recover the un-modeled accelerations rather well while GMP2b is the worst in the Y coordinate. Table 6 displays the statistics for the smoothing run. One can see that smoothing has greatly increased the recovery of un-modeled acclerations for case 2 as well.

Table 6. Case 2 fully observed period smoothed RMS Values. RMS values are computed from the difference between filtered estimates and true un-modeled accelerations. Percent change is calculated as GMP (RMS2 - RMS1)/RMS1.

	Position (m)					Acceleration (μm/s^2)				
	GMP1	GMP2a	%a	GMP2b	%b	GMP1	GMP2a	%a	GMP2b	%b
X	0.0167	0.0165	-1%	0.0251	50%	1.329	1.344	1%	3.001	126%
Y	0.0165	0.0180	9%	0.0280	70%	1.693	1.834	8%	3.277	94%
Z	0.1603	0.2004	25%	0.2617	63%	6.919	8.708	26%	10.722	55%
R	0.1620	0.2019	24%	0.2643	63%	7.245	8.999	24%	11.606	60%

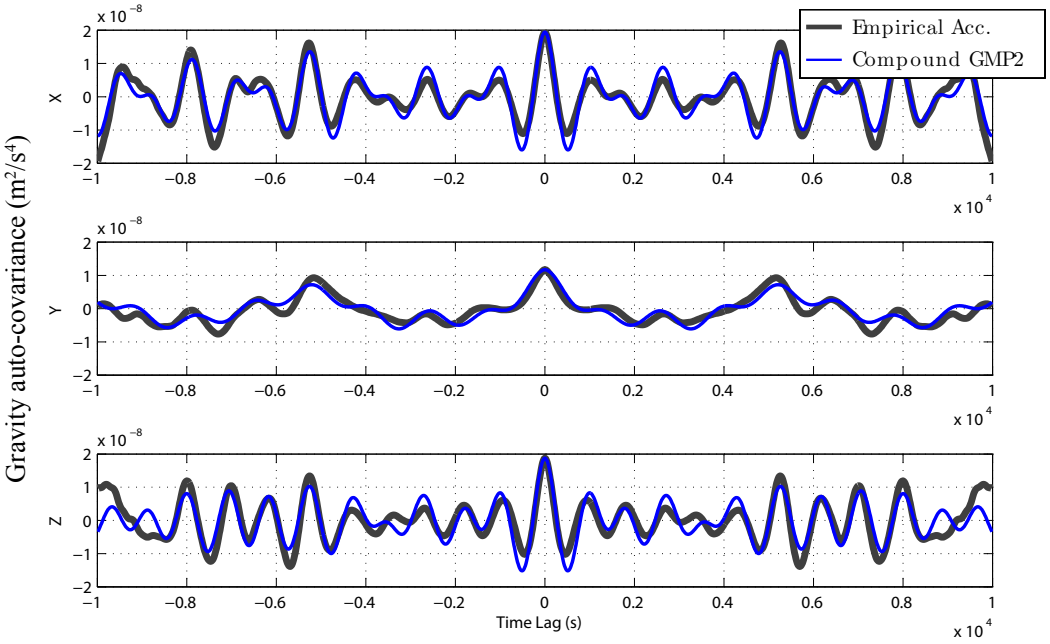

Figure 10. Compound GMP2: acceleration auto-covariance (gray) with compound GMP2 fit (blue).

Compound GMP2

As seen in the previous section, an optimal auto-covariance fit is necessary to accurately estimate and predict un-modeled accelerations. Here we attempt to use multiple GMP2s to achieve and optimal fit for the auto-covariance as seen in Figure 2. Figure 10 shows an auto-covariance fit of three compounded GMP2s. The three GMP2s are all of sinusoidal and oscillatory properties, in which the final GMP2 is forced to complete the auto-covariance fit near the origin. The filter performance resulting from the utilization of such a more complete auto-covariance fit should be fully assessed in the future

CONCLUSION

Summary

Empirical accelerations are commonly modeled with two extreme types of auto-covariance models in precise orbit determination: pure exponential decay or pure sinusoidal oscillation. A second-order Gauss-Markov process offers an auto-covariance model that is more flexible to fit against a wide variety of observed empirical behaviors. However, a trade-off may be necessary when one is attempting to fit a GMP2 auto-covariance to that of an empirical acceleration. One must not over-fit the auto-covariance in an attempt to obtain major frequencies at the expense of an optimal fit for small time-lags. In other words, an auto-covariance model that sustains oscillations at large time lags, instead of just dying off to zero, is a strong stochastic constraint that can be used to mitigate unobservability under poor tracking conditions. It must be used with restraint, though, for it may bias the filtering results in case the auto-covariance calibration is inaccurate.

We have demonstrated improvements in POD through the use of a GMP2 for modeling gravitational accelerations beyond J_2 that were un-modeled in the filter dynamic model. We have analyzed two cases in which empirical acceleration auto-covariances are highly variable. In both cases, the

use of a single well calibrated GMP2 outperformed a GMP1 and a poorly calibrated GMP2 for both continuous observations and poor tracking data.

It must be emphasized that an unrestrained auto-covariance fit has the potential to be more useful than a restrained one when observations are sparse. However, an unrestrained auto-covariance fit may also cause damage if it is inaccurate. In the case of dense observations, in which the system dynamics are already well constrained by the observations alone, it is advisable to avoid the risk of an inaccurate fit and adopt a more restrained auto-covariance fit.

Through the use of GMPs, increased filter performance led to more accurate estimates of the satellites position and acceleration having implications for gravity mapping missions such as CHAMP, GRACE, or GOCE as well as other science missions requiring precise orbit determination solutions. Through the use of a sequential filter and smoother, we have shown that properly calibrated GMPs can recover un-modeled accelerations better than a single sequential filter run.

Future Work

There are several avenues of future work to determine the applications of GMP2 for POD. There may be some cases in which handling empirical accelerations in other coordinate systems (e.g., RIC) will yield a more convenient auto-covariance model to fit a GMP2 to. However, the filter equations may become more complicated and it is not self-evident if the transformations of acceleration from frame to frame will be as trivial as those of position.

Another avenue of future work lies in applying GMP2s separately for accelerations of different physical origin that a satellite may encounter in orbit such as atmospheric drag, solar radiation pressure, or low-thrust maneuvers. Also, it may be better to estimate the parameters and coefficients driving the acceleration model instead of attempting to estimate the total empirical acceleration. Generally, this can only be done if certain parameters of the satellite are known.

Thirdly, the use of compounded GMPs needs to be investigated thoroughly to determine if they can improve POD and predictions. In this work we have seen how effective a single properly calibrated GMP can be when tracking data is dense. However, the best results were obtained when the time-lag fit of the GMP auto-covariance function was minimized based on the sparsity of tracking data. It is postulated that several GMPs can be used in combination to more accurately estimate un-modeled accelerations during large time gaps between observations and predictions.[7]

It would also be beneficial to derive GMP2 as a vector-valued processes and extend the analytical derivation to the full augmented system. This would allow for an accounting of cross-correlation between accelerations in different coordinates, which are currently neglected.

Finally, it is always desirable to use real tracking data to determine if GMP2 can increase the accuracy of position and acceleration estimation of a satellite. The addition of a GMP2 to such software as JPL's GYPSY-OASIS and GSFC's GEODYN will allow for such a comparison.

ACKNOWLEDGMENT

The second author acknowledges funding provided by Fulbright/Capes.

APPENDIX A: DERIVATION

There are two approaches to obtaining a solution to the theory of Gaussian random processes. The first is the method of Fokker-Planck or the diffusion equation method. The second pays attention to the actual random variation in time of system variables one is interested in. Here we follow the second. It is convenient to develop the interested variables in a Fourier time series of which the variable coefficients can vary in a random fashion. One of the basic theorems is the fundamental notion of the spectrum of the random process and the connection between the spectrum and correlation functions. Here we follow closely the derivation presented by References 9 and 10.

Suppose that we have a second-order differential equation which can be expressed in state vector notation as

$$\begin{bmatrix} \dot{x}_1 \\ \dot{x}_2 \end{bmatrix} = \begin{bmatrix} 0 & 1 \\ -\omega_n^2 & -2\zeta\omega_n \end{bmatrix} \begin{bmatrix} x_1 \\ x_2 \end{bmatrix} + \begin{bmatrix} 0 \\ c \end{bmatrix} w(t), \tag{31}$$

with a forcing function $w(t)$ which is a Gaussian random process with moments

$$\mathrm{E}\{w(t)\} = 0, \quad \mathrm{E}\{w(t)w(t+\tau)\} = q\delta(\tau). \tag{32}$$

The spectral density of $w(t)$ is the Fourier transform of the correlation function

$$S_w(\omega) = \int_{-\infty}^{\infty} dt e^{\mathrm{i}\omega t} \mathrm{E}\{w(t)w(0)\} = q, \tag{33}$$

which is white noise of strength q. We can take the Fourier transform of the state equations,

$$\begin{bmatrix} -\mathrm{i}\omega x_1(\omega) \\ -\mathrm{i}\omega x_2(\omega) \end{bmatrix} = \begin{bmatrix} 0 & 1 \\ -\omega_n^2 & -2\zeta\omega_n \end{bmatrix} \begin{bmatrix} x_1(\omega) \\ x_2(\omega) \end{bmatrix} + \begin{bmatrix} 0 \\ c \end{bmatrix} w(\omega), \tag{34}$$

then we can solve for $x_1(\omega)$ in terms of the fluctuating force to obtain

$$x_1(\omega) = \frac{c\, w(\omega)}{\omega_n^2 - \omega^2 - (2\zeta\omega_n)\mathrm{i}\omega}. \tag{35}$$

The spectral density of x_1 is proportional to $|x_1(\omega)|^2$ and so

$$S_{x_1}(\omega) = \frac{c^2 S_w(\omega)}{|\omega_n^2 - \omega^2 - (2\zeta\omega_n)\mathrm{i}\omega|^2} = \frac{c^2 q}{(\omega_n^2 - \omega^2)^2 + (2\zeta\omega_n)^2\omega^2}. \tag{36}$$

For the corresponding time dependent auto-covariance function we have

$$\Psi_{nn}(\tau) = \frac{1}{2\pi} \int_{-\infty}^{\infty} d\omega e^{-\mathrm{i}\omega t} S_{x_1}(\omega), \tag{37}$$

$$\Psi_{nn}(\tau) = \frac{qc^2}{4\omega_n^3\zeta} e^{-\zeta\omega_n|\tau|} \left\{ \cos\beta|\tau| + \frac{\zeta\omega_n}{\beta} \sin\beta|\tau| \right\}. \tag{38}$$

Next, the covariance matrix, $\bar{\mathbf{P}}_\mathrm{s}$, for purely a GMP2 (not the augmented system) is defined by

$$\bar{\mathbf{P}}_\mathrm{s}(t) = \Phi_\mathrm{s}(t, t_0)\mathbf{P}_\mathrm{s}(t_0)\Phi_\mathrm{s}^\mathrm{T}(t, t_0) + \int_{t_0}^{t} \Phi_\mathrm{s}(t, t')\mathbf{B}_\mathrm{s}(t')\mathbf{Q}_\mathrm{s}(t')\mathbf{B}_\mathrm{s}^\mathrm{T}(t')\Phi_\mathrm{s}^\mathrm{T}(t, t')dt', \tag{39}$$

where the state transition matrix for Eq. (31) is easily obtained:

$$\Phi_s(t) = e^{-\zeta\omega_n t}\begin{bmatrix} \cos\beta t + \dfrac{\zeta\omega_n}{\beta}\sin\beta t & \dfrac{1}{\beta}\sin\beta t \\ -\dfrac{\omega_n^2}{\beta}\sin\beta t & \cos\beta t - \dfrac{\zeta\omega_n}{\beta}\sin\beta t \end{bmatrix}, \tag{40}$$

with $\beta = \omega_n\sqrt{1-\zeta^2}$. Using $\mathbf{B}_{\mathrm{s}}(t') = [0,\ c]^{\mathrm{T}}$ and solving for $\bar{\mathbf{P}}_{\mathrm{s}}(t)$ yields

$$\begin{aligned} \bar{P}_{\mathrm{s}_{11}}(t) = e^{-2\zeta\omega_n t}\Bigg[&\left(\cos\beta t + \frac{\zeta\omega_n}{\beta}\sin\beta t\right)^2 \bar{P}_{\mathrm{s}_{11}}(0)\ldots \\ &+ \frac{2}{\beta}\sin\beta t\left(\cos\beta t + \frac{\zeta\omega_n}{\beta}\sin\beta t\right)\bar{P}_{s_{12}}(0) + \frac{1}{\beta^2}\sin^2\beta t\bar{P}_{\mathrm{s}_{22}}(0)\Bigg]\ldots \\ &+ \frac{qc^2}{4\omega_n^3\zeta}\left[1 - \frac{e^{-2\zeta\omega_n t}}{\beta^2}\left(\omega_n^2 - \zeta^2\omega_n^2\cos 2\beta t + \zeta\omega_n\beta\sin 2\beta t\right)\right], \end{aligned} \tag{41}$$

$$\begin{aligned} \bar{P}_{\mathrm{s}_{12}}(t) = e^{-2\zeta\omega_n t}\Bigg[&-\frac{\omega_n^2}{\beta}\sin\beta t\left(\cos\beta t + \frac{\zeta\omega_n}{\beta}\sin\beta t\right)\bar{P}_{\mathrm{s}_{11}}(0)\ldots \\ &+ \left(\cos^2\beta t - \frac{1+\zeta^2}{1-\zeta^2}\sin^2\beta t\right)\bar{P}_{\mathrm{s}_{12}}(0)\ldots \\ &+ \frac{1}{\beta}\sin\beta t\left(\cos\beta t - \frac{\zeta\omega_n}{\beta}\sin\beta t\right)\bar{P}_{\mathrm{s}_{22}}(0)\Bigg]\ldots \\ &+ \frac{qc^2}{2\beta^2}e^{-2\zeta\omega_n t}\sin^2\beta t, \end{aligned} \tag{42}$$

$$\begin{aligned} \bar{P}_{\mathrm{s}_{22}}(t) = e^{-2\zeta\omega_n t}\Bigg[&\frac{\omega_n^2}{1-\zeta^2}\left(\sin^2\beta t\right)\bar{P}_{\mathrm{s}_{11}}(0)\ldots \\ &- \frac{2\omega_n^2}{\beta}\sin\beta t\left(\cos\beta t - \frac{\zeta\omega_n}{\beta}\sin\beta t\right)\bar{P}_{\mathrm{s}_{12}}(0)\ldots \\ &+ \left(\cos\beta t - \frac{\zeta\omega_n}{\beta}\sin\beta t\right)^2\bar{P}_{\mathrm{s}_{22}}(0)\Bigg]\ldots \\ &+ \frac{qc^2}{4\omega_n\zeta}\left[1 - \frac{e^{-2\zeta\omega_n t}}{\beta^2}\left(\omega_n^2 - \zeta^2\omega_n^2\cos 2\beta t + \zeta\omega_n\beta\sin 2\beta t\right)\right]. \end{aligned} \tag{43}$$

From the solutions given in Eq. (41) thru Eq. (43), the correlation matrix can be obtained for the statistically stationary state and is given by:

$$\begin{bmatrix}\Psi_{11} & \Psi_{12}\\ \Psi_{21} & \Psi_{22}\end{bmatrix} = \frac{qc^2}{4\omega_n^3\zeta}e^{-\zeta\omega_n|\tau|}\begin{bmatrix} \cos\beta|\tau| + \dfrac{\zeta\omega_n}{\beta}\sin\beta|\tau| & \dfrac{\omega_n^2}{\beta}\sin\beta|\tau| \\ \dfrac{\omega_n^2}{\beta}\sin\beta|\tau| & \cos\beta|\tau| - \dfrac{\zeta\omega_n^3}{\beta}\sin\beta|\tau| \end{bmatrix}. \tag{44}$$

We would like for $\mathrm{E}\{x_{\mathrm{s}}^2(t)\} = \sigma^2$ as $t\to\infty$, so the desired value of c^2 is

$$c^2 = \frac{4\omega_n^3\zeta\sigma^2}{q}. \tag{45}$$

APPENDIX B: IMPLEMENTATION

Here we assist the interested reader in implementing the above model into a sequential Kalman filter and briefly describe the structure of the main matrices and vectors involved. This is an extension of the implementation presented in Reference 7. Let the position vector of the satellite state in three-dimensional space be defined as $\mathbf{r} = [x,\ y,\ z]^{\mathrm{T}}$ and let the velocity vector be $\dot{\mathbf{r}} = [\dot{x},\ \dot{y},\ \dot{z}]^{\mathrm{T}}$. The satellite state $\mathbf{X}$ contains the position and velocity vectors as well as p parameters describing drag, gravity, etc., defined by $\boldsymbol{\beta}$ where:

$$\mathbf{X} = \begin{bmatrix}\mathbf{r}^{\mathrm{T}} & \dot{\mathbf{r}}^{\mathrm{T}} & \boldsymbol{\beta}^{\mathrm{T}}\end{bmatrix}^{\mathrm{T}}. \tag{46}$$

The shaping-filter state vector $\mathbf{X}_{\mathrm{s}}$ is made up of two vectors, $\mathbf{X}_{\mathrm{s}_1}$ and $\mathbf{X}_{\mathrm{s}_2}$, each with three spatial dimensions:

$$\mathbf{X}_{\mathrm{s}} = \begin{bmatrix}\mathbf{X}_{\mathrm{s}_1}^{\mathrm{T}} & \mathbf{X}_{\mathrm{s}_2}^{\mathrm{T}}\end{bmatrix}^{\mathrm{T}} = \begin{bmatrix}X_{\mathrm{s}_1 x} & X_{\mathrm{s}_1 y} & X_{\mathrm{s}_1 z} & X_{\mathrm{s}_2 x} & X_{\mathrm{s}_2 y} & X_{\mathrm{s}_2 z}\end{bmatrix}^{\mathrm{T}}. \tag{47}$$

The augmented state vector can then be defined as $\mathbf{X}_{\mathrm{a}} = \begin{bmatrix}\mathbf{X}^{\mathrm{T}},\ \mathbf{X}_{\mathrm{s}}^{\mathrm{T}}\end{bmatrix}^{\mathrm{T}}$ with a state rate vector given as:

$$\dot{\mathbf{X}}_{\mathrm{a}} = \begin{bmatrix}\dot{\mathbf{r}}_{\mathrm{a}}^{\mathrm{T}} & \ddot{\mathbf{r}}_{\mathrm{a}}^{\mathrm{T}} & \dot{\boldsymbol{\beta}}^{\mathrm{T}} & \mathbf{X}_{\mathrm{s}_2}^{\mathrm{T}} & (-\boldsymbol{\omega}_n^2 \circ \mathbf{X}_{\mathrm{s}_1} - 2\boldsymbol{\zeta} \circ \boldsymbol{\omega}_n \circ \mathbf{X}_{\mathrm{s}_2})^{\mathrm{T}}\end{bmatrix}^{\mathrm{T}}. \tag{48}$$

Notice that there can be three spatial dimensions given to the GMP2 parameter vectors $\boldsymbol{\sigma}$, $\boldsymbol{\omega}_n$, and $\boldsymbol{\zeta}$, for example $\boldsymbol{\zeta} = [\zeta_x,\ \zeta_y,\ \zeta_z]^{\mathrm{T}}$; in other words, a separate GMP2 process is used for each coordinate. The operation $\boldsymbol{\zeta} \circ \boldsymbol{\omega}_n = [\zeta_x \omega_{nx},\ \zeta_y \omega_{ny},\ \zeta_z \omega_{nz}]^{\mathrm{T}}$ is the element-wise product of two vectors. Vector exponentiation is defined element-wise: $\boldsymbol{\omega}_n^2 = [\omega_{nx}^2,\ \omega_{ny}^2,\ \omega_{nz}^2]^{\mathrm{T}}$. Augmented accelerations are thus defined as $\ddot{\mathbf{r}}_{\mathrm{a}} = \ddot{\mathbf{r}} + \ddot{\mathbf{r}}_{\mathrm{s}}$ where $\ddot{\mathbf{r}}$ are the deterministic dynamic model accelerations (i.e. gravity, atmospheric drag, etc.) and $\ddot{\mathbf{r}}_{\mathrm{s}}$ are the empirical accelerations from the shaping filter output, $\ddot{\mathbf{r}}_{\mathrm{s}} = \mathbf{X}_{\mathrm{s}_1}$. The augmented velocities are defined as $\dot{\mathbf{r}}_{\mathrm{a}}$ and are simply related to the integration of $\ddot{\mathbf{r}}_{\mathrm{a}}$.

The $\mathbf{A}_{\mathrm{a}}(t)$ matrix is the Jacobian of the augmented state-rate with respect to the augmented state and has the following partitioning:

$$\begin{aligned}\mathbf{A}_{\mathrm{a}}(t) &= \begin{bmatrix}\mathbf{A}(t) & \mathbf{B}(t)\tilde{\mathbf{H}}_{\mathrm{s}}(t) \\ \mathbf{0}_{6\times(6+p)} & \mathbf{A}_{\mathrm{s}}(t)\end{bmatrix} \\ &= \begin{bmatrix}\mathbf{0} & \mathbf{I} & \dfrac{\partial \dot{\mathbf{r}}}{\partial \boldsymbol{\beta}} & \mathbf{0} & \mathbf{0} \\ \dfrac{\partial \ddot{\mathbf{r}}}{\partial \mathbf{r}} & \dfrac{\partial \ddot{\mathbf{r}}}{\partial \dot{\mathbf{r}}} & \dfrac{\partial \ddot{\mathbf{r}}}{\partial \boldsymbol{\beta}} & \mathbf{I} & \mathbf{0} \\ \dfrac{\partial \dot{\boldsymbol{\beta}}}{\partial \mathbf{r}} & \dfrac{\partial \dot{\boldsymbol{\beta}}}{\partial \dot{\mathbf{r}}} & \dfrac{\partial \dot{\boldsymbol{\beta}}}{\partial \boldsymbol{\beta}} & \mathbf{0} & \mathbf{0} \\ \mathbf{0} & \mathbf{0} & \mathbf{0}_{3\times p} & \mathbf{I} & \mathbf{0} \\ \mathbf{0} & \mathbf{0} & \mathbf{0}_{3\times p} & -\mathrm{diag}(\boldsymbol{\omega}_n \circ \boldsymbol{\omega}_n) & -2\,\mathrm{diag}(\boldsymbol{\zeta} \circ \boldsymbol{\omega}_n)\end{bmatrix}\end{aligned} \tag{49}$$

Except where noted, the identity matrix $\mathbf{I}$ and null matrix $\mathbf{0}$ have the dimensions 3-by-3. The matrix $\tilde{\mathbf{H}}_{\mathrm{s}}(t) = [\mathbf{I},\ \mathbf{0}]^{\mathrm{T}}$ which comes from $\mathbf{X}_{s_1}$ being the shaping filter output. The matrix $\mathbf{B}(t) = [\mathbf{0},\ \mathbf{I} = \partial \ddot{\mathbf{r}}_{\mathrm{s}} / \partial \mathbf{X}_{\mathrm{s}_1},\ \mathbf{0}_{p\times 3}]^{\mathrm{T}}$ comes from $\mathbf{X}_{\mathrm{s}_1}$ being the acceleration in the same coordinate as $\ddot{\mathbf{r}}_{\mathrm{s}}$.

The augmented $\tilde{\mathbf{H}}_{\mathrm{a}}(t)$ matrix is the Jacobian of the observations with respect to the augmented state and is simply:

$$\tilde{\mathbf{H}}_{\mathrm{a}}(t) = \begin{bmatrix} \tilde{\mathbf{H}}(t) & \mathbf{0}_{m\times 6} \end{bmatrix}^{\mathrm{T}}, \tag{50}$$

where none of the m scalar range and range-rate observations depend on the empirical accelerations. The matrix $\mathbf{B}_{\mathrm{a}}(t)$ is the Jacobian of the state-rate with respect to the white noise and is given as:

$$\mathbf{B}_{\mathrm{a}}(t) = \begin{bmatrix} \mathbf{0}_{(6+p)\times 3} \\ \mathbf{B}_{\mathrm{s}}(t) \end{bmatrix} = \begin{bmatrix} \mathbf{0}_{(6+p)\times 3} \\ \mathbf{0} \\ \mathrm{diag}(\mathbf{c}) \end{bmatrix}, \tag{51}$$

where c is determined from Eq. (45).

The state-transition matrix $\Phi_{\mathrm{a}}(t, t_0)$ can be obtained from numerical integration of $\mathbf{A}_{\mathrm{a}}(t)$ with the initial conditions $\Phi_{\mathrm{a}}(t_0, t_0) = \mathbf{I}$. Here we have used an efficient seventh-order Ruge-Kutta-Fehlberg RKF7(8) algorithm to numerically integrate Φ_{a}. One may also use the analytical expressions for the Φ-matrix as seen in Eq. (40).

The time-updated state covariance matrix can be obtained two different ways. The first is numerical integration of Eq. (18). The other is for the discrete case given in Eq. (19) where the covariance matrix can be broken up into two terms: $\bar{\mathbf{P}}_{\mathrm{a}} = \bar{\mathbf{P}}'_{\mathrm{a}} + \bar{\mathbf{P}}''_{\mathrm{a}}$; the first term is simply $\bar{\mathbf{P}}'_{\mathrm{a}} = \Phi_{\mathrm{a}}\mathbf{P}_{\mathrm{a}}\Phi_{\mathrm{a}}^{\mathrm{T}}$; and the second term:

$$\bar{\mathbf{P}}''_{\mathrm{a}} = \mathbf{B}_{\mathrm{d}}(t_0)\mathbf{Q}_{\mathrm{d}}(t_0)\mathbf{B}_{\mathrm{d}}^{\mathrm{T}}(t_0) = \mathbf{B}_{\mathrm{d}}(t_0)\left[\mathbf{B}_{\mathrm{a}}(t_0)\mathbf{Q}_{\mathrm{a}}(t_0)\mathbf{B}_{\mathrm{a}}^{\mathrm{T}}(t_0) \times (t - t_0)\right]\mathbf{B}_{\mathrm{d}}^{\mathrm{T}}(t_0). \tag{52}$$

Some simplifications for this case can be made as discussed in Reference 8 in which we postulate that $\mathbf{B}_{\mathrm{d}} = \mathbf{I}$, $\mathbf{Q}_{\mathrm{a}} = \mathbf{I}$, resulting in:

$$\bar{\mathbf{P}}''_{\mathrm{a}} = \begin{bmatrix} \mathbf{0}_{(6+p)\times(6+p)} & \mathbf{0}_{(6+p)\times 3} & \mathbf{0}_{(6+p)\times 3} \\ \mathbf{0}_{3\times(6+p)} & \mathbf{0} & \mathbf{0} \\ \mathbf{0}_{3\times(6+p)} & \mathbf{0} & \mathrm{diag}(\mathbf{c}\circ\mathbf{c}) \end{bmatrix} \times |t - t_0|, \tag{53}$$

where the absolute value surrounding the time-lag is necessary when running the filter in a backwards manner, such as a sequential smoother. It must be emphasized that Eq. (52) and Eq. (53) are first order approximations and are only valid if the system model is time-invariant or slowly varying. If the system is not time-invariant or slowly varying an analytical solution or numerical integration of Eq. (18) is necessary. It may also be necessary to obtain an analytical solution or numerical integration of Eq. (18) if one is making future predictions in which time-lags are considerably large.

REFERENCES

[1] S. Luthcke, N. Zelensky, D. Rowlands, F. Lemoine, and T. Williams, "The 1-Centimeter Orbit: Jason-1 Precision Orbit Determination Using GPS, SLR, DORIS, and Altimeter Data Special Issue: Jason-1 Calibration/Validation," *Marine Geodesy*, Vol. 26, No. 3, 2003, pp. 399–421.

[2] S. Wu, T. Yunck, and C. Thornton, "Reduced-dynamic technique for precise orbit determination of low earth satellites," *Astrodynamics 1987*, Vol. 1, 1988, pp. 101–113.

[3] O. Montenbruck, T. Van Helleputte, R. Kroes, and E. Gill, "Reduced dynamic orbit determination using GPS code and carrier measurements," *Aerospace Science and Technology*, Vol. 9, No. 3, 2005, pp. 261–271.

[4] J. Marshall, N. Zelensky, S. Klosko, D. Chinn, S. Luthcke, K. Rachlin, and R. Williamson, "The temporal and spatial characteristics of TOPEX/POSEIDON radial orbit error," *Journal of geophysical research*, Vol. 100, No. C12, 1995, pp. 25331–25.

[5] K. Myers and B. Tapley, "Dynamical model compensation for near-earth satellite orbit determination," *AIAA Journal*, Vol. 13, 1975, pp. 343–349.

[6] B. Tapley, B. Schutz, and G. Born, *Statistical Orbit Determination*. Academic Press, 2004.

[7] F. G. Nievinski, B. Yonko, and G. H. Born, "Improved orbit determination using second-order Gauss-Markov processes," *AAS/AAIA Space Flight Mechanics Meeting*, New Orleans, Louisiana, February 13-17 2011. AAS 11-119.

[8] P. Maybeck, *Stochastic models, estimation and control*, Vol. 141-1. Academic press, 1979.

[9] A. Bryson and Y. Ho, *Applied optimal control: optimization, estimation, and control*. Hemisphere Pub, 1975.

[10] M. Wang and G. Uhlenbeck, "On the theory of the Brownian motion II," *Reviews of Modern Physics*, Vol. 17, No. 2-3, 1945, pp. 323–342.

[11] E. Fehlberg, *Classical fifth-, sixth-, seventh-, and eighth-order Runge-Kutta formulas with stepsize control*. National Aeronautics and Space Administration; for sale by the Clearinghouse for Federal Scientific and Technical Information, Springfield, Va., 1968.

[12] B. Tapley, J. Ries, S. Bettadpur, D. Chambers, M. Cheng, F. Condi, B. Gunter, Z. Kang, P. Nagel, R. Pastor, T. Pekker, S. Poole, and F. Wang, "GGM02 - An improved Earth gravity field model from GRACE," *Journal of Geodesy*, 2005. DOI 10.1007/s00190-005-0480-z.

[13] R. G. Gottlieb, "Fast Gravity, Gravity Partials, Normalized Gravity, Gravity Gradient Torque and Magnetic Field: Derivation, Code and Data," Tech. Rep. NASA Contractor Report 188243, NASA Lyndon B. Johnson Space Center, Houston, TX, Feb 1993.

[14] J. Picone, A. Hedin, D. Drob, and A. Aikin, "NRLMSISE-00 empirical model of the atmosphere: Statistical comparisons and scientific issues," *Journal of Geophysical Research*, Vol. 107, No. A12, 2002, p. 1468.

[15] P. Maybeck, *Stochastic models, estimation and control*, Vol. 141-2. Academic press, 1979.

[16] B. Kovačević and Z. Durovic, *Fundamentals of stochastic signals, systems and estimation theory with worked examples*. Springer Verlag, 2008.

[17] J. Crassidis and J. Junkins, *Optimal estimation of dynamic systems*, Vol. 2. Chapman & Hall, 2004.

[18] J. Speyer and W. Chung, *Stochastic processes, estimation, and control*, Vol. 17. Society for Industrial & Applied, 2008.